Proceedings of the IASS 2024 Symposium
Redefining the Art of Structural Design
August 26-30, 2024, Zurich Switzerland
Philippe Block, Giulia Boller, Catherine DeWolf,
Jacqueline Pauli, Walter Kaufmann (eds.)

Structural Form-finding Integrating Vector-based Graphic Statics and Non-Linear Force Density Method

Yuchi SHEN[a*], Yinan XIAO[b*], Feifan HE[c], Pierluigi D'ACUNTO[cd]

[a*] Southeast University, School of Architecture
Sipailou 2#, Nanjing, China
yuchi_shen@seu.edu.cn
[b*] Technische Universität Braunschweig, Institute of Structural Design
Pockelsstraße 4, 38106 Braunschweig, Germany
yinan.xiao@tu-braunschweig.de

[c] Technical University of Munich, Germany, TUM School of Engineering and Design, Department of Architecture, Professorship of Structural Design
[d] Technical University of Munich, Germany, TUM Institute for Advanced Study

Abstract

This paper presents a novel workflow for form-finding that sequentially integrates Vector-based Graphic Statics (VGS) and the Non-Linear Force Density Method (NLFDM) to address form-finding and nonlinear optimization challenges in structural design. The NLFDM typically necessitates appropriate initial force densities and boundary conditions to prevent degenerate outcomes, excelling in solving nonlinear optimizations. Besides, VGS can effectively achieve static equilibrium through interdependent form and force diagrams. The proposed integrated approach relies on the following steps: Initially, VGS transforms designer-specified structures into topologically valid form and force diagrams, enforcing interdependency between corresponding edges in the two diagrams using a parallelization algorithm. When the VGS produces a staged solution closer to the equilibrium than the input, the workflow transitions to NLFDM, adjusting the force densities of both diagrams to reach static equilibrium while fulfilling user-defined design constraints. This interplay between VGS and NLFDM ensures stability and reduces the occurrence of degenerate solutions. The approach is validated through one case study of a tension-compression structure.

Keywords: form-finding, Vector-based Graphic Statics, Non-Linear Force Density Method, structural optimization, form diagram, force diagram.

1. Introduction

Vector-based Graphic Statics (VGS) (D'Acunto et al. [1]) and the Force Density Method (FDM) (Linkwitz and Schek [2], and Schek [3]) are computational form-finding approaches for the design of spatial network structures in static equilibrium [4]. While both methods are material-independent and focus on geometric stiffness (Veenendaal et al. [5]), their inputs and computational approaches differ. The present research focuses on integrating VGS and NLFDM to enhance the form-finding capabilities of the individual methods and align with nonlinear design-constrained optimization tasks. This integration leverages the strengths of each method: NLFDM requires suitable initial conditions and excels in nonlinear optimizations, while VGS achieves static equilibrium under linear constraints.

1.1. Vector-based Graphic Statics

VGS uses graphical constructions to create a force diagram from any form diagram with an underlying planar or non-planar graph (D'Acunto et al. [1]). The form diagram represents the geometry of the structure and its applied loads, whereas the force diagram shows the static equilibrium of the structure through closed cycles of force vectors that represent the forces applied on the structure's nodes. For static

equilibrium to be achieved, the edges in the form diagram must be parallel to their corresponding force vectors in the force diagram. By modifying the force diagram, the form diagram transforms accordingly under a set of geometric constraints to achieve equilibrium and vice versa (D'Acunto et al. [6]). Form-finding occurs during this interdependent transformation between the two diagrams. Static equilibrium states are explored for specific load conditions in kinematically indeterminate systems, not necessarily for stabilized structural networks under multiple load cases. Various strategies have been explored to achieve equilibrium. The recently released VGS toolkit (Jasienski et al. [7]) used Kangaroo2 (Piker [8]) to facilitate an interactive form-finding process. The underlying principle relies on a projection-based dynamic relaxation solver (Bouaziz et al. [9]), which entails projecting particles onto constraints and cyclically adjusting to equilibrium in a pseudo-dynamic system with damping. An alternative method is an algebraic-based approach that utilizes a parallelization algorithm (Avelino et al. [10]) based on a least-squares solution (Traa [11]).

1.2. Non-Linear Force Density Method

FDM simplifies nonlinear equilibrium equations for unknown positions of free nodes in a structure into linear equations by introducing the force-to-length ratio as force density. To incorporate constraints for specific design targets, extended methods (i.e. Non-Linear Force Density Method (NLFDM)) were introduced by Schek (1974) [3], Malerba et al. (2012) [12], and Aboul-Nasr and Mourad (2015) [13] to impose further constraints to the FDM. These methods iteratively adjust the input force densities through a gradient-based optimization procedure that meets the specific design goals with constraints.

VGS and NLFDM may face challenges in highly nonlinear optimization contexts, especially when dealing with tension-compression structures, risking entrapment in local optima or leading to degenerate solutions. In the current computational implementation of VGS (Jasienski et al. [7]), geometric and mechanical constraints can be easily described. However, the convergence speed is relatively slow compared to gradient-based optimization. Moreover, the form-finding result is highly sensitive to the initial status. Unreasonable initial conditions may lead to unstable convergence. The algebraic-based approach provides a clear mathematical framework with light computational resource requirements [14]. However, it is currently limited to handling linear constraints or objective functions. In NLFDM, when the input force densities significantly differ from the force densities in the final equilibrium structure, or in cases where structural optimization problems are non-convex global optimization challenges, the algorithm often converges to local optima, failing to identify solutions that satisfy all input design constraints (Malerba et al. [12]). Besides, the algorithm produces degenerate results when encountering singular matrix issues, especially in self-stressed structures. Addressing this issue necessitates additional strategies, such as minimizing an objective function of virtual work and pre-defining the length of compression (Miki et al. [15]) or analyzing the force densities using Singular Value Decomposition (SVD) (Pellegrino [16]).

1.3. Objective and contribution

The present research focuses on combining VGS and NLFDM to further broaden the solution range of both methods. The NLFDM requires appropriate initial force densities and boundary conditions to avoid degenerate outcomes and excels in solving nonlinear optimizations. VGS is a general geometric-based method that can effectively achieve static equilibrium and fulfill the linear constraints by imposing the geometric features of the form and force diagrams. Therefore, the two methods can provide a better starting point for each other, compensating for their respective limitations. In this regard, exploring a hybrid framework could significantly enhance form-finding capabilities and effectively align with nonlinear design-constrained optimization tasks.

1.4. Nomenclature

Table 1: Nomenclature of the concepts used in this paper

Category	Symbol	Description
Diagram	$\boldsymbol{F}$	Form diagram.

	$\boldsymbol{F}^*$	Force diagram.
	$\widehat{\boldsymbol{F}}^*$	Initial force diagram (not necessarily representing an equilibrium state).
Graph	$\widetilde{\boldsymbol{F}}$	Underlying (directed) graph of the form diagram.
	$\widetilde{\boldsymbol{F}}^*$	Underlying (directed) graph of the force diagram.
Matrix	$\boldsymbol{C}$	Edge-node incidence matrix in $[e \times v]$.
	$\boldsymbol{C}_s$	Subspace in $\boldsymbol{C}$ that contains the internal force elements and nodes exclusively
	$\boldsymbol{C}^*$	Edge-vertex incidence matrix in $[e \times v^*]$.
Parameters	$\boldsymbol{q}$	Force density [N/m] vector of a structure.
	$\boldsymbol{P}$	Set of loads [N] applying at the nodes of a structure.
	L	Set of lengths [m] of all the elements in a structure.
	LP	Load path [N·m] of a structure [17].
	Int. nodes	Indices of intermittent fixed nodes (fixed in NLFDM and released in VGS).
Linear Constraints	IP	Constraining specific vertices of a structure to lie on a defined plane Ω.
	EL	Constraining specific elements of a structure to have equal length.
	FM	Constraining specific elements of a structure to have a given force magnitude.
Nonlinear Objectives	$min.LP$	Objective of minimizing the load path of a structure.

2. Integration of VGS and NLFDM

2.1. Data-structure

The link between VGS and NLFDM requires a shared data structure to synchronize their interplay mechanism. An incidence matrix $\boldsymbol{C}([e \times v])$ is used to depict the directed graph $\widetilde{\boldsymbol{F}}$ of a form diagram $\boldsymbol{F}$ in VGS with e number of edges and v number of nodes. This matrix is formed by augmenting $\boldsymbol{C}_s$ with additional columns that indicate the end nodes of external force vectors and by adding extra rows to account for the edges related to the external forces (Fig. 1). Based on $\boldsymbol{C}$, the matrix $\boldsymbol{C}^*([e \times v^*])$ for the directed graph $\widetilde{\boldsymbol{F}}^*$ of force diagram $\boldsymbol{F}^*$ can be built up, as described by Van Mele et al. [14]. This graph contains as many v^* nodes as faces in $\widetilde{\boldsymbol{F}}$, and the same number of edges e as in $\widetilde{\boldsymbol{F}}$. The column vectors of $\boldsymbol{C}^*$ is generated from $\widetilde{\boldsymbol{F}}$ by cycling its faces in a counter-clockwise direction [14]. For each *j-th* column of $\boldsymbol{C}^*$, the component c_{ij}^* is 1 if *i-th* edge is adjacent to the *j-th* face and is oriented in the same direction as the counter-clockwise cycle around the face in $\widetilde{\boldsymbol{F}}$, -1 if opposite, and 0 if the edge is not adjacent to that face. After implementing the data-structure to describe the form and force diagram, the structure attains a compatible data format that connects the topology information in both VGS and NLFDM.

2.2. Form-finding Workflow

In the proposed form-finding workflow (Fig. 2), VGS imposes the geometric interdependency between form and force diagrams while approaching the locally linear constraints: *IP*, *EL,* and *FM*. NLFDM is initialized using the result produced by VGS, and it optimizes for the nonlinear objective: *min. LP*. Three indicators are defined to evaluate the form-finding results: the static equilibrium (*R*), the extent to which all the linear constraints (*IP*, *EL,* and *FM*) are fulfilled (*ε*), and to which the *LP* [17] is minimized. The constraints and objectives are met when these three indicators are near zero, i.e., within the specified tolerance (*t*). These indicators are formulated as follows:

$$R = \sum_{i=1}^{n} \cos^{-1}\left(\frac{\boldsymbol{u}_i \boldsymbol{v}_i}{|\boldsymbol{u}_i||\boldsymbol{v}_i|}\right), \tag{1}$$

$$\varepsilon = \boldsymbol{r}^T \boldsymbol{r}, \tag{2}$$

$$\Delta LP = |LP_n - LP_k|, \tag{3}$$

where $\boldsymbol{u}_i, \boldsymbol{v}_i$ are the corresponding pairs of the *i*-th edge's direction vectors in $\boldsymbol{F}$ and $\boldsymbol{F}^*$. $\boldsymbol{r}$ is the residual vector of the constraints.

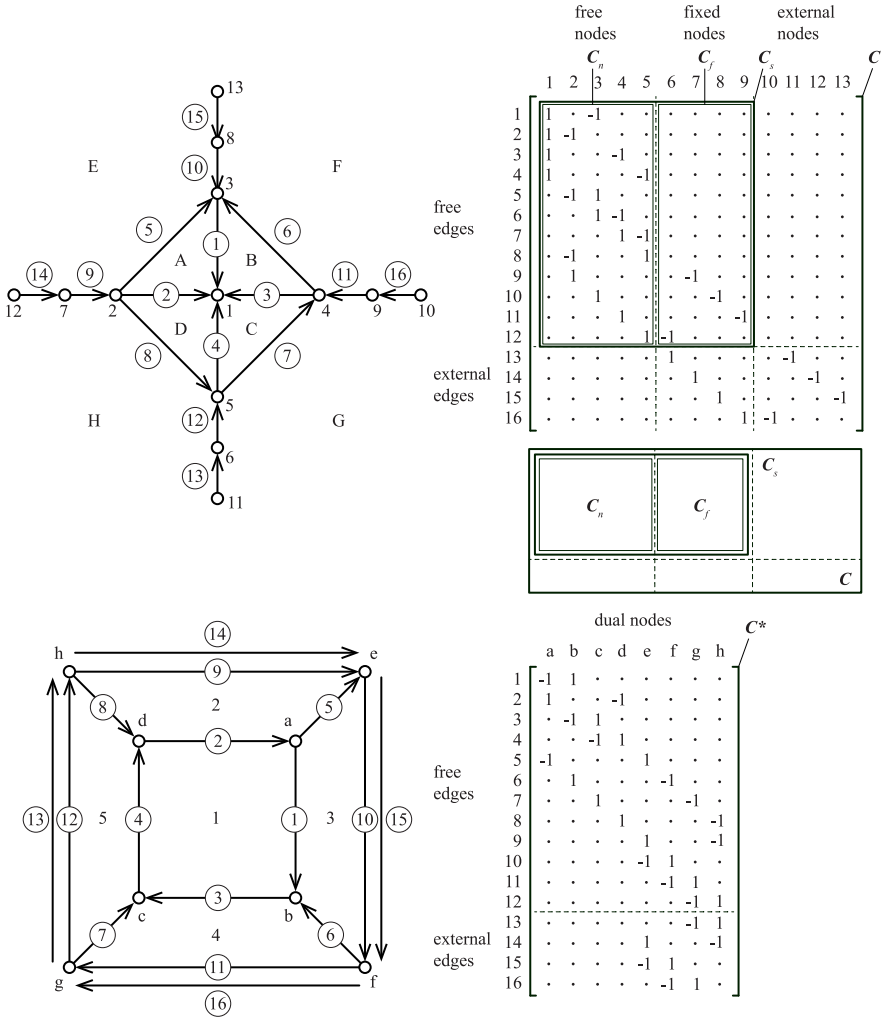

Figure 1: Left column: topologies of form and force diagram are interpreted as directed graphs $\widetilde{\boldsymbol{F}}$ and $\widetilde{\boldsymbol{F}}^*$. Right column: matrices of form and force diagrams that synchronize the data-structure between VGS and FDM.

Initialization: As shown in Fig. 2, the workflow starts with the initial form diagram $\boldsymbol{F}_0$ derived from the user-defined input. The $\widetilde{\boldsymbol{F}}^*$ is built based on the underlying graph $\widetilde{\boldsymbol{F}}$. Given predefined applied loads $\boldsymbol{P}$, initial $\boldsymbol{q}$, linear constraints, and the fixed geometry of $\boldsymbol{F}_0$, the parallelization algorithm (Avelino et al. [10]) in VGS is used to adjust the force diagram $\widetilde{\boldsymbol{F}}^*$ towards equilibrium. It is important to note that the fixed geometry of the initial $\boldsymbol{F}_0$ may prevent $\widetilde{\boldsymbol{F}}^*$ from achieving exact equilibrium. Nonetheless, this initial step provides an effective foundation for the subsequent iterative steps.

Iterative steps: Using $\boldsymbol{P}$, $\boldsymbol{C}_s$, $\boldsymbol{F}_0$, the updated $\boldsymbol{q}$, and the support nodes as inputs to the NLFDM, the optimization process considers the gradient of the combined constraints and integrates it with the gradient of the design goal function. Thus, the objective function becomes to minimize a mixture of finite increments of difference of $\boldsymbol{q}$ and $\boldsymbol{r}$, as well as the *Load Path* (*LP*) with variable weights: $min.\ w_1(\Delta \boldsymbol{q}^T \Delta \boldsymbol{q} + \boldsymbol{r}^T \boldsymbol{r}) + w_2(LP)$. The NLFDM produces an equilibrium solution but not necessary fulfils all constraints. Taking over the updated $\boldsymbol{F}_i$, and $\boldsymbol{F}_i^*$, VGS further imposes the geometric interdependency between the form and force diagrams using the parallelization algorithm (PA, $\boldsymbol{e}^{//}()$). This procedure adjusts the form based on the *IP*, *EL* and *FM* constraints and updates the form and force

diagrams to $\boldsymbol{F}_k$ and $\boldsymbol{F}_k^*$. This state fulfills the linear constraints and the equilibrium but not necessarily the user-defined nonlinear goals. Therefore, $\boldsymbol{F}_k$, $\boldsymbol{F}_k^*$, and $\boldsymbol{q}_k$ become the input to the NLFDM for a new round of gradient-based optimization for nonlinear goals with the updated boundary conditions, producing $\boldsymbol{F}_n$ and $\boldsymbol{F}_n^*$. The *iterative steps* are repeated until both sets of constraints are met ($R, \varepsilon < t$), and the difference of the objective function values in two algorithms is less than the tolerance ($|LP_n - LP_k| < t$). The nodes of the structure that can only move in VGS and are fixed in NLFDM are labeled as *intermittent fixed nodes* (*int. nodes*).

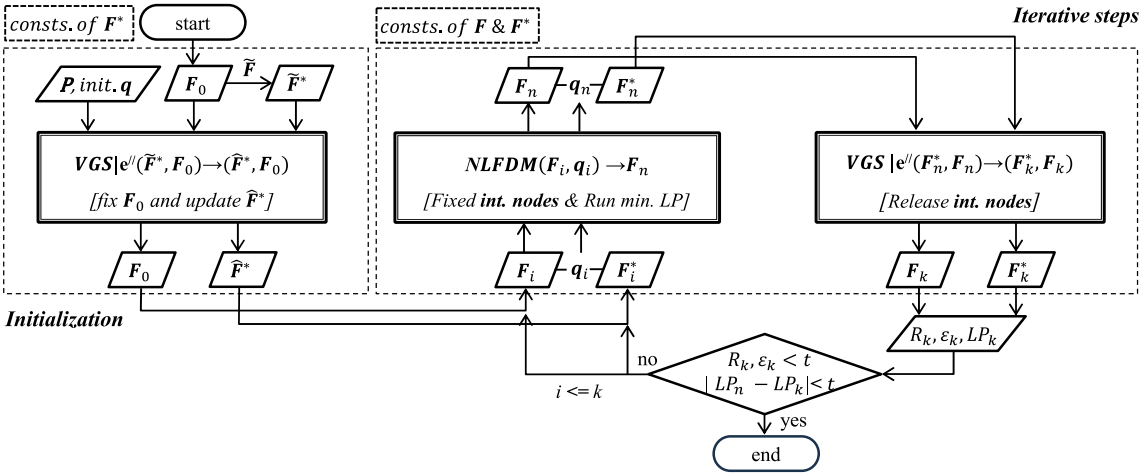

Figure 2: The flowchart of the integrated workflow of VGS and NLFDM.

3. Case study: a hexagonal prism tensegrity

3.1. Initial setup and optimization goal

A benchmark task is established to test the proposed form-finding workflow, as shown in Fig. 3. The structure consists of a hexagonal prism tensegrity with 12 nodes and 24 edges. Initial internal forces of 10kN and -10kN in magnitude are assigned to the tensile and compressive members, respectively. The goal is to find the form that minimizes the *Load Path* (*min. LP*) subject to the following constraints:

a. In-plane constraints (*IP*): the top nodes $\{V_0, V_1, ..., V_5\}$ can freely move within a plane Ω_1, while the bottom nodes $\{V_6, V_7, ..., V_{11}\}$ are fixed in the plane Ω_2.

b. Equal length constraints (*EL*): the length set $\{l_{0\text{-}1}, l_{1\text{-}2}, \ldots, l_{5\text{-}0}\}$ of the top edge elements should be equal and must exceed 5m; additionally, the two length sets $\{l_{0\text{-}6}, l_{1\text{-}7}, \ldots, l_{5\text{-}11}\}$ and $\{l_{0\text{-}11}, l_{1\text{-}6}, \ldots, l_{5\text{-}10}\}$ of the middle elements should each have equal lengths within their respective sets.

c. Force magnitude constraints (*FM*): Forces in the vertical elements must be equal to -20N.

The form-finding process relies on two hypotheses: it focuses exclusively on the static equilibrium for the given loading conditions, excluding stability considerations; the self-weight of the structure is ignored, as it is considered negligible compared to the internal pre-stressing forces.

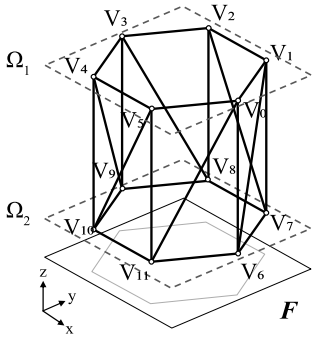

min. LP (non-linear)

IP: V_0 - V_5 on Ω_1; V_6 - V_{11} on Ω_2 and fixed

EL: $l_{01} = l_{12} = l_{23} = l_{34} = l_{45} = l_{50} >= 5$m; $l_{011} = l_{16} = l_{27} = l_{38} = l_{49} = l_{510}$; $l_{06} = l_{17} = l_{28} = l_{39} = l_{410} = l_{511}$

FM: $f_{011} = f_{16} = f_{27} = f_{38} = f_{49} = f_{510} = -20$N

Figure 3: The nonlinear optimization problem applied to a hexagonal prism tensegrity structure.

3.2. Form-finding using only VGS

The use of the sole VGS with the parallelization algorithm for form-finding highlights this method's limitation. Starting from the state of ***F*** in Fig. 3, the optimization stalled at the state shown in Fig. 4 with an *LP* of 6058.10 N·m. It achieved a static equilibrium solution (R = 5.559e-6) but did not optimize *min. LP*, because nonlinear goals cannot be formulated within the algorithm.

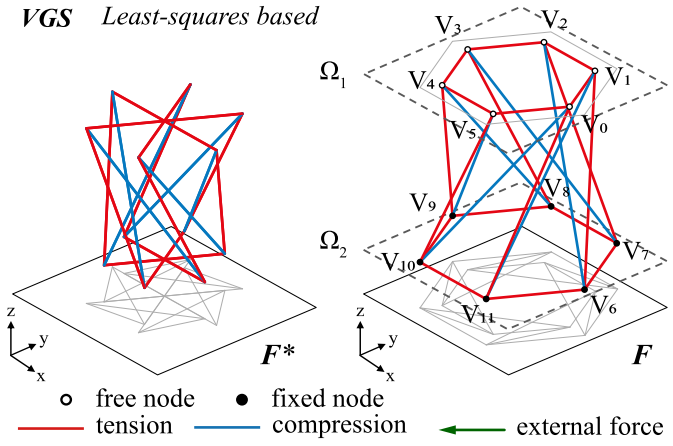

input:	init $\boldsymbol{q}$; $\boldsymbol{C}_s$.
obj. :	min. $\Delta\boldsymbol{q}^{\mathrm{T}}\bullet\Delta\boldsymbol{q}$.
const.:	fixed nodes: V_6 - V_{11}, *IP*: V_0 - V_5 on Ω_1, *EL*: three groups in Fig. 1, *FM*: f_{011} - f_{510} = 20N, $\boldsymbol{e} \parallel \boldsymbol{e}^*$,
iter.:	75.
res.:	R = 5.56e-6, ε = 0.00, *LP* = 6058.10 N·m. *min. LP cannot be formulated!*

Figure 4: The benchmark test with VGS parallelization

3.3. Form-finding using only NLFDM

As shown in Fig. 5, when only the bottom vertices {V_6, V_7, ..., V_{11}} are set as fixed nodes in the NLFDM, a singular solution (ε = 2032.56) is generated. The model can further incorporate V_5 to achieve a valid solution (See Fig. 6) with ε = 143.48, meaning the linear constraints cannot be fulfilled while fixing the extra vertex V_5. NLFDM is not always effective in form-finding tasks with flexible boundary conditions, leading to singular matrix issues, as highlighted by Miki et al. [15] and Pellegrino [16]. It may also perform poorly when initiated with an initial force density set that is far from the target, as discussed by Malerba et al. [12].

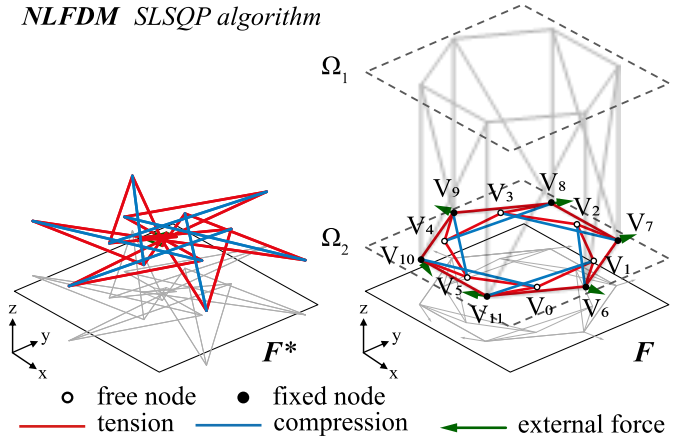

input:	init $\boldsymbol{q}$; $\boldsymbol{C}_s$; fixed nodes: V_6 - V_{11}.
obj. :	min. $w_1(\Delta\boldsymbol{q}^{\mathrm{T}}\bullet\Delta\boldsymbol{q} + \boldsymbol{r}^{\mathrm{T}}\bullet\boldsymbol{r}) + w_2(LP)$.
const.:	*IP*: V_0 - V_5 on Ω_1, *EL*: three groups in Fig. 1, *FM*: f_{011} - f_{510} = 20N, reaction forces: rf_6 - rf_{11} = 0, bounds of $\boldsymbol{q}$,
iter.:	57.
res.:	R = 0.00, ε = 2032.34, *LP* = 3062.92 N·m. *Degenerated solution occurs!*

Figure 5: The benchmark test with NLFDM, in which only the V_6-V_{11} are fixed.

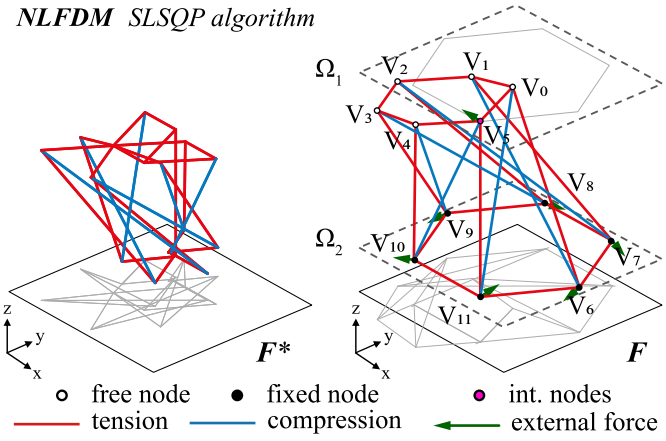

input	: init $\boldsymbol{q}$; $\boldsymbol{C}_s$; fixed nodes: V_6 - V_{11}, V_5.
obj.	: min. $w_1(\Delta \boldsymbol{q}^T \cdot \Delta \boldsymbol{q} + \boldsymbol{r}^T \cdot \boldsymbol{r}) + w_2(LP)$.
const.	: *IP*: V_0 - V_4 on Ω_1, *EL*: three groups in Fig. 1, *FM*: f_{011} - f_{510} = 20N, reaction forces: rf_6 - rf_{11}, rf_5= 0, bounds of $\boldsymbol{q}$,
iter.	: 24.
res.	: R = 0.00, ε = 142.41, LP = 5704.16 N·m. *Constraints cannot be fulfilled!*

Figure 6: The benchmark test with NLFDM, in which the V_6-V_{11} and V_5 (as the ***int. node***) are fixed.

3.4. Form-finding through VGS + NLFDM

This section illustrates the application of the proposed VGS + NLFDM workflow described in Section 2 to the benchmark test case.

Initialization: The input for the form-finding process includes the form diagram $\boldsymbol{F}$, the list of force densities $\boldsymbol{q}$ defined by the user, as well as the incidence matrix $\boldsymbol{C}$ derived from $\boldsymbol{F}$. Since the choice of the initial $\boldsymbol{q}$ is crucial in the gradient-based optimization process, an initialization strategy is applied to ensure the optimized result aligns closely with the user's input. As illustrated in Fig. 7, a force diagram $\boldsymbol{F}^*$ is generated, which is topologically connected with $\boldsymbol{F}$ but does not fulfill the condition of parallelism between the diagrams. Consequently, the parallelization algorithm is applied in VGS, the $\boldsymbol{F}^*$ transforms according to the constraints (*IP*, *EL*) related to $\boldsymbol{F}$, and the constraints (*FM*) related to $\boldsymbol{F}^*$. Through the transformation, $\boldsymbol{F}$ and $\boldsymbol{F}^*$ turned to $\boldsymbol{F}'$ and $\boldsymbol{F}^{*\prime}$ tending toward the equilibrium state but without reaching it. The $\boldsymbol{q}'$ derived from $\boldsymbol{F}'$ and $\boldsymbol{F}^{*\prime}$ is closer to an equilibrium configuration than the input $\boldsymbol{q}$. Therefore, $\boldsymbol{F}'$,$\boldsymbol{F}^{*\prime}$, and $\boldsymbol{q}'$ provide a starting point for the subsequent process.

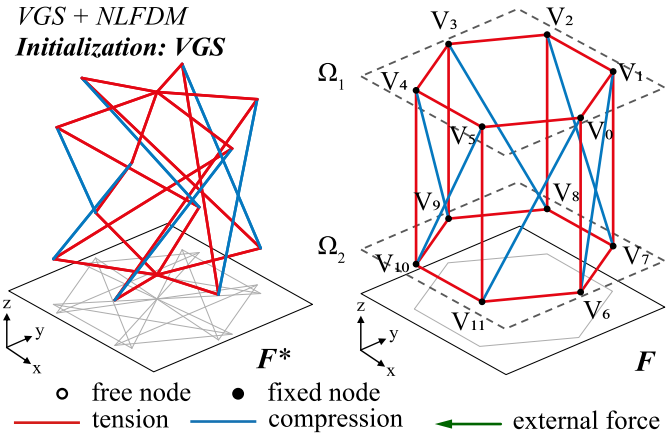

input	: init $\boldsymbol{q}$; $\boldsymbol{C}_s$; init $\boldsymbol{F}$.
obj.	: min. $\Delta \boldsymbol{q}^T \cdot \Delta \boldsymbol{q}$.
const.	: fixed $\boldsymbol{F}$, *FM*: f_{011} - f_{510} = 20N, $\boldsymbol{e} \parallel \boldsymbol{e}^*$,
iter.	: 3.
res.	: R = 15.00, ε = 142.41, LP = 6932.90 N·m. *Constraints cannot be fulfilled!* *min. LP cannot be formulated!*

Figure 7: The initialization of the VGS+NLFDM framework.

Iterative steps: After the initialization process, the nodes in the structure are categorized into two types: free nodes (V_0 – V_4) and fixed nodes (V_5 - V_{11}), in which *int. node* V_5 is fixed in NLFDM but released in VGS. Both types, along with the initialized list of force densities $\boldsymbol{q}'$, the matrix $\boldsymbol{C}$ and the constraints (Fig. 8), are fed into the NLFDM algorithm. Solving the nonlinear objective function (*min. LP*) in NLFDM with fixed *int. node* may prevent the fulfillment of certain constraints (Fig. 8 step 1a). The form-finding process then switches to VGS (Fig. 8 step 1b). During this phase, the *int. node* V_5 is released to impose inter-parallelism and linear constraints between the two diagrams. Subsequently, a new iteration between NLFDM and VGS is started to approach the global optimal solution. After several iterations, the form-finding objectives and constraints are satisfied (Fig. 8 step 2).

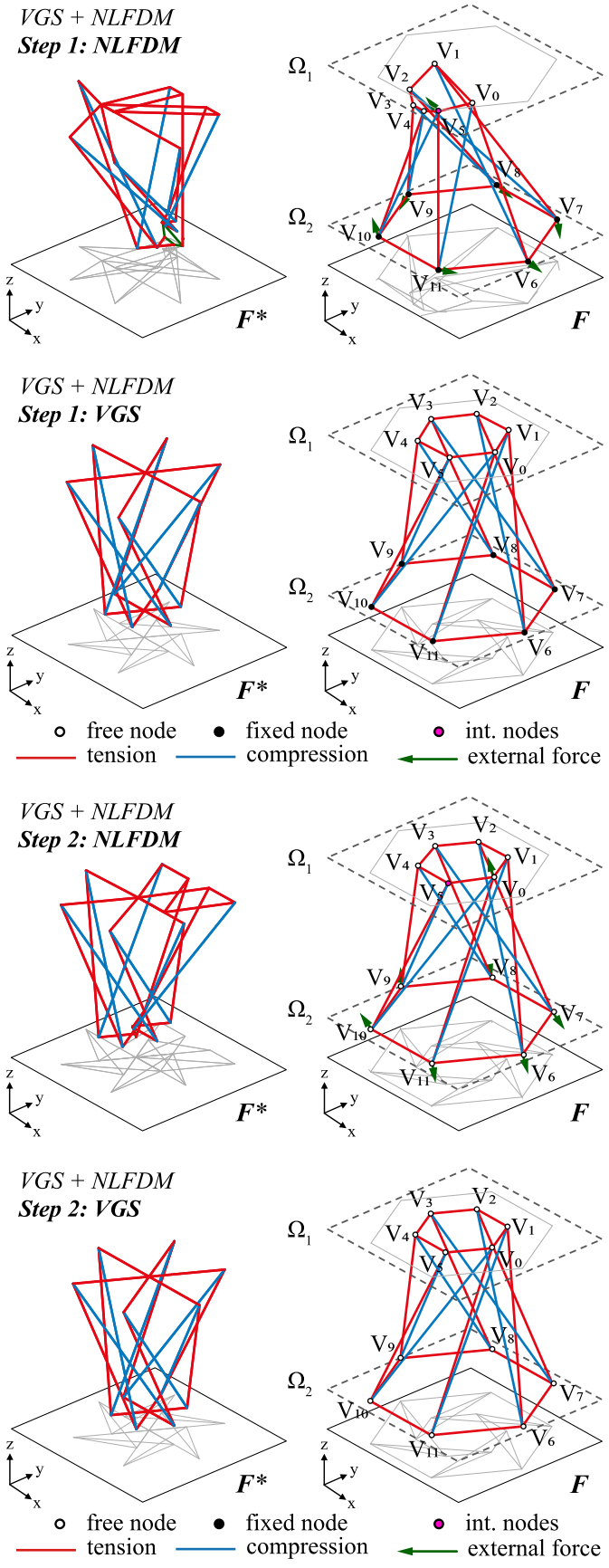

input: init $\boldsymbol{q}$; $\boldsymbol{C}_s$; fixed nodes: V_6 - V_{11}, V_5.
obj. : min. $w_1(\Delta\boldsymbol{q}^T\cdot\Delta\boldsymbol{q} + \boldsymbol{r}^T\cdot\boldsymbol{r}) + w_2(LP)$.
const.: *IP*: V_0 - V_4 on Ω_1,
EL: three groups in Fig. 1,
FM: f_{011} - f_{510} = 20N,
reaction forces: rf_6 - rf_{11}, rf_5= 0,
bounds of $\boldsymbol{q}$,
iter.: 52.
res.: R = 0.00,
ε = 156.69,
LP = 6014.88 N·m.
Constraints cannot be fulfilled!

input: updated $\boldsymbol{q}$; $\boldsymbol{C}_s$.
obj. : min. $\Delta\boldsymbol{q}^T\cdot\Delta\boldsymbol{q}$.
const.: fixed node: V_6 - V_{11},
IP: V_0 - V_5 on Ω_1,
EL: three groups in Fig. 1,
FM: f_{011} - f_{510} = 20N,
$\boldsymbol{e} \parallel \boldsymbol{e}^*$,
iter.: 95.
res.: R = 1.90e-5,
ε = 0.00,
LP = 5752.61 N·m.

min. LP cannot be formulated!

input: init $\boldsymbol{q}$; $\boldsymbol{C}_s$; fixed nodes: V_6 - V_{11}, V_5.
obj. : min. $w_1(\Delta\boldsymbol{q}^T\cdot\Delta\boldsymbol{q} + \boldsymbol{r}^T\cdot\boldsymbol{r}) + w_2(LP)$.
const.: *IP*: V_0 - V_4 on Ω_1,
EL: three groups in Fig. 1,
FM: f_{011} - f_{510} = 20N,
reaction forces: rf_6 - rf_{11}, rf_5= 0,
bounds of $\boldsymbol{q}$,
iter.: 25.
res.: R = 0.00,
ε = 0.054,
LP = 5742.57 N·m.
Constraints cannot be fulfilled!

input: updated $\boldsymbol{q}$; $\boldsymbol{C}_s$.
obj. : min. $\Delta\boldsymbol{q}^T\cdot\Delta\boldsymbol{q}$.
const.: fixed node: V_6 - V_{11},
IP: V_0 - V_5 on Ω_1,
EL: three groups in Fig. 1,
FM: f_{011} - f_{510} = 20N,
$\boldsymbol{e} \parallel \boldsymbol{e}^*$,
iter.: 5.
res.: R = 2.50e-6,
ε = 0.00,
LP = 5754.62 N·m.

Figure 8: The iterative steps of the integrated VGG and NLFDM workflow. In Step 1a, NLFDM optimizes *min. LP* but fails to retain the linear constraints because of the fixed V_5; In Step 1b, the VGS only fulfills the

equilibrium and linear constraints but does not minimize the Load Path; In Step 2a NLFDM searches the optimal solution with the updated fixed V_5; In Step 2b, VGS further relaxes the form and force diagrams, and the location of V5 does not change. The values of ΔLP, R, ε are all smaller than the tolerance.

The case study demonstrates that integrating VGS and NLFDM methods effectively addresses specific form-finding problems that each method struggles with individually. VGS excels at solving equilibrium problems and adhering to linear constraints but cannot handle nonlinear objectives. Conversely, NLFDM effectively tackles nonlinear objectives through gradient-based optimization but requires certain nodes to be fixed, limiting its applicability. The integrated methods overcome these limitations.

4. Conclusion

This research introduced a form-finding workflow that merges VGS with NLFDM. By implementing the parallelization algorithm proposed by Avelino et al. [10] in the VGS framework (D'Acunto et al. [1], Jasienski et al. [7]) using an enhanced matrix data-structure based on Algebraic Graph Statics (Van Mele et al. [14]), the proposed workflow effectively addresses nonlinear design-constrained optimization challenges and prevent the risk of local optima and degenerate solutions in tension-compression structures. The efficacy of this approach was demonstrated through a case study, illustrating the synergistic effects of VGS and NLFDM. Future research should further explore the following aspects:

Enhancing data structure for non-planar graphs: The proposed workflow enhanced the data structure introduced by the Algebraic Graph Statics framework (Van Mele et al. [14]) to adapt to the VGS framework. The data structure should be further extended to cover the case of 3D structures with underlying non-planar graphs.

Constraint-based parallelization: Methods should be investigated to steer the parallelization algorithm toward fulfilling design constraints while achieving static equilibrium.

Automatic differentiation: Implementing Automatic Differentiation (AD) will be investigated to further optimize the gradient-informed form-finding methods in VGS and NLFDM, as demonstrated in the case of Combinatorial Equilibrium Modelling [18].

Acknowledgments

Yuchi Shen received support from the Natural Science Foundation of China (NSFC#52208010) and the China Postdoctoral Science Foundation (#2022M720716). Yinan Xiao received support from Matthäi - Stiftung, Germany. Feifan He acknowledges the support of China Scholarship Council program (No.202206120041).

References

[1] P. D'Acunto, J. P. Jasienski, P. O. Ohlbrock, C. Fivet, J. Schwartz, and D. Zastavni, "Vector-based 3D graphic statics: A framework for the design of spatial structures based on the relation between form and forces," *Int J Solids Struct*, vol. 167, pp. 58–70, Aug. 2019, doi: 10.1016/j.ijsolstr.2019.02.008.

[2] K. Linkwitz and H.-J. Schek, "Einige Bemerkungen zur Berechnung von vorgespannten Seilnetzkonstruktionen," Springer-Verlag, 1971.

[3] H. J. Schek, "The force density method for form finding and computation of general networks," *Comput Methods Appl Mech Eng*, vol. 3, no. 1, pp. 115–134, Jan. 1974, doi: 10.1016/0045-7825(74)90045-0.

[4] G. Boller and P. D'Acunto, "Structural design via form finding: Comparing Frei Otto, Heinz Isler and Sergio Musmeci," in *History of Construction Cultures*, London: CRC Press, 2021, pp. 431–438. doi: 10.1201/9781003173434-168.

[5] D. Veenendaal and P. Block, "An overview and comparison of structural form finding methods for general networks," *Int J Solids Struct*, vol. 49, no. 26, pp. 3741–3753, Dec. 2012, doi: 10.1016/j.ijsolstr.2012.08.008.

[6] P. D'Acunto, J. P. Jasienski, P. O. Ohlbrock, and C. Fivet, "Vector-Based 3D Graphic Statics: Transformations of Force Diagrams," in *Proceedings of IASS Annual Symposium*, Hamburg, Germany: Proceedings of the IASS Annual Symposium 2017.

[7] J. P. Jasienski, Y. Shen, P. O. Ohlbrock, D. Zastavni, and P. D'Acunto, "A Computational implementation of Vector-based 3D Graphic Statics (VGS) for interactive and real-time structural design," *Computer-Aided Design*, vol. 171, no. 103695, May 2024, doi: 10.1016/j.cad.2024.103695.

[8] D. Piker, "Kangaroo2." Accessed: Apr. 14, 2024. [Online]. Available: https://www.food4rhino.com/en/app/kangaroo-physics

[9] S. Bouaziz, S. Martin, T. Liu, L. Kavan, and M. Pauly, "Projective Dynamics: Fusing Constraint Projections for Fast Simulation," in *Seminal Graphics Papers: Pushing the Boundaries, Volume 2*, New York, NY, USA: ACM, 2023, pp. 787–797. doi: 10.1145/3596711.3596794.

[10] R. M. Avelino, J. Lee, T. Van Mele, and P. Block, "An interactive implementation of algebraic graphic statics for geometry-based teaching and design of structures," in *fib Symposium*, fib. The International Federation for Structural Concrete, 2021, pp. 447–454. doi: 10.35789/fib.PROC.0055.2021.CDSymp.P054.

[11] J. Traa, "Least-Squares Intersection of Lines." University of Illinois at Urbana-Champaign, 2013. [Online]. Available: https://docplayer.net/21072949-Least-squares-intersection-of-lines.html

[12] P. G. Malerba, M. Patelli, and M. Quagliaroli, "An Extended Force Density Method for the form finding of cable systems with new forms," *Structural Engineering and Mechanics*, vol. 42, no. 2, pp. 191–210, Apr. 2012, doi: 10.12989/sem.2012.42.2.191.

[13] G. Aboul-Nasr and S. A. Mourad, "An extended force density method for form finding of constrained cable nets," *Case Studies in Structural Engineering*, vol. 3, pp. 19–32, Jun. 2015, doi: 10.1016/j.csse.2015.02.001.

[14] T. Van Mele and P. Block, "Algebraic graph statics," *Computer-Aided Design*, vol. 53, pp. 104–116, Aug. 2014, doi: 10.1016/j.cad.2014.04.004.

[15] M. Miki and K. Kawaguchi, "Extended force density method for form finding of tension structures," *Journal of International Association for Shell and Spatial Structures*, vol. 51, no. 4, pp. 291–303, 2010.

[16] S. Pellegrino, "Structural Computations with the Singular Value Decomposition of the Equilibrium Matrix," *Int J Solids Struct*, vol. 30, pp. 3025–3035, 1993, doi: https://doi.org/10.1016/0020-7683(93)90210-X.

[17] P. O. Ohlbrock, P. D'Acunto, J. P. Jasienski, and C. Fivet, "Vector-based 3D graphic statics (part III): designing with Combinatorial Equilibrium Modelling," in *Proceedings of IASS Annual Symposium 2016*, Tokyo, 2016.

[18] R. Pastrana, P. O. Ohlbrock, T. Oberbichler, P. D'Acunto, and S. Parascho, "Constrained Form-Finding of Tension–Compression Structures using Automatic Differentiation," *Computer-Aided Design*, vol. 155, p. 103435, Feb. 2023, doi: 10.1016/j.cad.2022.103435.